

Keck Spectroscopy of Red Giant Stars in the Vicinity of M31's Massive Globular Cluster G1¹

David B. Reitzel

Department of Physics & Astronomy, 8371 Mathematical Sciences Building, University of California at Los Angeles, Los Angeles, California 90095, USA

reitzel@astro.ucla.edu

Puragra Guhathakurta

UCO/Lick Observatory, University of California at Santa Cruz, 1156 High Street, Santa Cruz, California 95064, USA

raja@ucolick.org

and

R. Michael Rich

Department of Physics & Astronomy, 8371 Mathematical Sciences Building, University of California at Los Angeles, Los Angeles, California 90095, USA

rmr@astro.ucla.edu

ABSTRACT

We present results from an ongoing Keck spectroscopic survey of red giant stars in a field located along the major axis of M31, ≈ 34 kpc in projection from the nucleus and near the luminous globular cluster G1. We use multislit LRIS spectroscopy to measure the Ca II near-infrared triplet in 41 stars ranging in apparent magnitude from $20 < I < 22$. Of these, 23 stars are found to have radial velocities $v < -200$ km s⁻¹ indicating that they are giants in M31; the rest are likely to be foreground Galactic dwarf stars. Roughly two-thirds of the M31 members concentrate at $v = -451$ km s⁻¹, with a relatively small velocity spread [$\sigma(\text{Gaussian}) = 27$ km s⁻¹] which suggests that they belong to the outer disk or possibly a cold debris trail in the halo. The mean velocity of this group of red giants is consistent with that of nearby neutral hydrogen and models of the velocity field of M31's disk, rather than with G1 or the systemic velocity of M31. We use V, I photometry to estimate a mean metallicity of $\langle [\text{Fe}/\text{H}]_{\text{phot}} \rangle = -0.8$ for this group of potential M31 outer disk stars. Six stars out of the 23 M31 member giants have metallicities and velocities consistent with those of G1 (after accounting for its intrinsic spread in v and $[\text{Fe}/\text{H}]$): one of these stars lies within the projected tidal radius of G1 and is a likely member; the remaining 5 stars are not physically close to G1, and may represent tidal debris from G1. However, more data are needed to confirm the nature of these 5 stars, as it is likely that they simply represent M31's field halo population. We might have expected to detect tidal debris if G1 were the remnant core of a dwarf galaxy being accreted by M31; instead, the majority of M31 giants in this field are metal-rich and belong to what is evidently the outer disk of M31, and only a small fraction ($\lesssim 20\%$) could possibly have originated in G1.

Subject headings: galaxies: individual: Andromeda galaxy [Messier 31 (M31), NGC 224, UGC 454, CGCG 535-017] – galaxies: formation – stars: red giants – stars: metallicity – clusters: globular: G1

1. Introduction

The outer regions of M31 have become an increasingly complicated field of study as it has become clear in recent years that the role of accretion in halo formation is of considerable importance. Ferguson et al. (2002) present star-count maps showing what appear to be extensive tidal disturbances in the halo of M31, including in the vicinity of the massive globular cluster G1. Reitzel & Guhathakurta (2002, hereafter RG02) find evidence for a subtle stream-like feature, in an outer halo field located 19 kpc from the center in projection along the southeastern minor-axis, using a combination of kinematics and metallicity measurements of red giant branch (RGB) stars. Guhathakurta & Reitzel (2002) confirm that this feature continues along the minor axis in two inner halo fields located near the globular clusters G312 and G302, located 11 and 7 kpc from the nucleus of M31 respectively near the southeastern minor axis. M31’s two closest satellites M32 and NGC 205 are known to be undergoing tidal stripping (Choi, Guhathakurta, & Johnston 2002); yet there is no definite proposal for a companion that might have been responsible for the large-scale streams seen in the halo.

The area around G1 is a particularly interesting field to study, as this object has been proposed to be the core of a tidally-disrupted dwarf galaxy (Meylan et al. 2001). If this is the case, one might expect to find the tidal debris surrounding the main body of the object with velocities and metallicities similar to G1 itself. In addition, the field around G1 is expected to have roughly equal numbers of M31 halo and disk stars (Reitzel, Guhathakurta, & Gould 1998; Hodder 1995) so this gives us the opportunity to study the disk population of M31 further out ($r \sim 34$ kpc) than has been done to date. Ferguson & Johnson (2001) study a field 30 kpc from the nucleus of M31 along the NE major axis and estimate a mean metallicity of $[\text{Fe}/\text{H}] \simeq -0.7$; they find that the population is mostly old (> 8 Gyr) but there is evidence for an intermediate-age population as well. In a paper that accompanies this work, Rich et al. (2003) report evidence for an intermediate-age population (6–8 Gyr) only 2 kpc from the location of G1. Davidge (2003) examines the outer disks of NGC 2403 and M33 and finds evidence for an intermediate-age population well outside the current star-forming disk in both galaxies.

The observations (imaging and spectroscopy), data reduction, and analysis are presented in § 2, a discussion follows in § 3, and a summary in § 4.

¹Data presented herein were obtained at the W. M. Keck Observatory, which is operated as a scientific partnership among the California Institute of Technology, the University of California and the National Aeronautics and Space Administration. The Observatory was made possible by the generous financial support of the W. M. Keck Foundation.

2. Observations and Data Analysis

2.1. Imaging/Stellar Photometry

The Low Resolution Imaging Spectrograph (LRIS; Oke et al. 1995) on the Keck II 10-m telescope is used in both imaging and spectroscopic modes for this project. The LRIS imaging data were obtained on August 15, 1998 (UT) and consist of single 5-min exposures in the V and I bands centered on the globular cluster G1. The seeing FWHM was about $0.8''$ and the sky conditions photometric. The 2048×1600 pixel images cover $7.3' \times 5.7'$ with a pixel scale of $0.215''$. After standard initial processing of the data—2D overscan subtraction, trimming, flat fielding, and fringe removal (in the I -band only), the DAOPHOT software package (Stetson 1987) is used for object detection and (V , I) photometry. Star-galaxy separation is done on the basis of image morphology. Several astrometric standard stars from the USNO Catalog happen to lie on our LRIS images and this allows for accurate calibration of the stellar (x , y) positions into (α , δ) coordinates.

Archival *Hubble Space Telescope*² (*HST*)/Wide Field Planetary Camera 2 (WFPC2) images from programs GO-5464 and GO-5907, two pointings centered on G1 but at different telescope roll angles, are also analyzed. Each pointing consists of images in the F555W and F814W bands (roughly equivalent to the V and I bands, respectively), with total exposure times per band of 1660 and 1280 s (GO-5464) and 2200 and 1800 s (GO-5907). The WFPC2 images are processed through the standard *HST* pipeline, and the HSTphot package (Dolphin 2000) is used to obtain a list of stellar positions and (V , I) photometry on the Johnson/Cousins system based on the transformation relations of Holtzman et al. (1995).

The agreement in stellar magnitudes between the two WFPC2 pointings is better than 0.1 mag, and the measurements are averaged for stars common to both pointings. The WFPC2 pointings are contained entirely within the LRIS imaging field and cover only its central portion. The LRIS V and I magnitude zeropoints are adjusted to match WFPC2 photometry using stars in the overlap region; the rms difference between WFPC2 and (adjusted) LRIS magnitudes is 0.1 mag. Stellar photometry with WFPC2 is somewhat more accurate than with LRIS, so the former is used wherever possible ($\sim 30\%$ of the final sample of stars).

2.2. Spectroscopy

A sample of 57 spectroscopic targets in the apparent magnitude range $20 < I < 22$ were selected from the above stellar photometry/astrometry list. Two multi-slit masks were designed using Drew Phillips' `simulator` software, one having 30 slitlets and the other 27 slitlets on M31 RGB star candidates, with the targets distributed more-or-less uniformly over the LRIS field of view. Multi-slit spectroscopic observations were carried using Keck/LRIS during a two-night run on September 28–29, 1998 (UT). Each spectrum covers the spectral range $\lambda\lambda 7550\text{--}8850 \text{ \AA}$ containing the near-infrared Ca II triplet: $\lambda\lambda 8498$, 8542 , and 8662 \AA . The instrumental spectral/velocity resolution is $1.94 \text{ \AA}/68 \text{ km s}^{-1}$ (FWHM); see RG02 for details. The total exposure times for the two masks is 1.7 and 2.0 hr. Individual exposures are typically 30 min long, although some exposures were stopped short due to telescope, instrument, and weather problems.

Overscan correction, 2D bias structure subtraction, and cosmic ray removal are accomplished using

²Based on observations made with the NASA/ESA Hubble Space Telescope obtained at the Space Telescope Science Institute, which is operated by the Association of Universities for Research in Astronomy, Inc., under NASA Contract NAS 5-2655.

standard IRAF³ tasks. Cosmic rays are removed on the basis of object sharpness and peak pixel brightness. They are masked from each image along with a surrounding 1-pixel buffer to remove the low-level wings of each event. A flat-field correction for each data frame is performed using a spectral dome flat that is well-matched to the data frame in terms of LRIS flexure effects. Data reduction issues/complications for LRIS spectra are discussed in some detail in RG02; that study did not however use the Phillips et al. (2003) reduction software that is used here.

Wavelength calibration, sky subtraction and extraction are all accomplished using the LRIS data reduction pipeline developed by Phillips et al. (2003). The software uses an optical model for the various elements of the LRIS spectrograph (collimator, grating, camera, etc.) to derive a mapping from the slitmask to the CCD detector as a function of wavelength. This optical model is based on spectrograph design drawings, and has been empirically refined using calibration spectra (arc lamp through a grid-of-holes mask) taken close to the observing run to account for misalignment of any of LRIS' elements. Even so the model is only good to about 0.3 pixels (0.06'' in the spatial direction and $\sim 0.2\text{\AA}$ in the dispersion direction). In addition, one must allow for small time-dependent alignment/focus errors, and variations from exposure to exposure because of instrument flexure. These errors are removed by low-order corrections: a zeropoint correction in wavelength measured from a bright night-sky emission line, and a plate-scale and offset which are solved for using the measured locii of slitlet edges.

2.3. Radial Velocity Measurement

In order to determine the radial velocity of each object, its final coadded spectrum is cross-correlated against a template spectrum (average spectrum of three control sample stars from RG02, where the coaddition is done after shifting each to zero velocity). The cross-correlation function (CCF) is computed from -1000 to $+1000$ km s⁻¹, covering a plausible range of radial velocities for stars associated with M31. The CCF technique yields an unambiguous peak and a reliable radial velocity for 41 of the 57 objects comprising the main sample of potential M31 targets. A complete description of this CCF procedure is given in RG02.

The radial velocity determined from the location of the CCF peak, v_{obs} , is corrected to the heliocentric frame using the task RVCOR in IRAF. We estimate the rms error in radial velocity from the degree of significance of the CCF peak: $\sigma_v = \sigma_v^{\text{TD}}(1 + r_{\text{TD}})^{-1}$ (Tonry & Davis 1979). The value of σ_v^{TD} is empirically found to be 77 km s⁻¹ for our instrumental set-up (RG02). The mean 1σ error in velocity for this G1 field sample is 21 km s⁻¹.

The success rate for radial velocity measurements in our sample is 41 out of 57, or about 72%. This is somewhat lower than the 80% success rate in the RG02 study, but the difference can be attributed to two factors:

1. RG02 estimate that less than half their failures, about 7% of the spectroscopic sample, are background field galaxies. The surface density of M31 giants is probably higher near G1 ($r \sim 34$ kpc, major axis) than in RG02's field ($r \sim 19$ kpc, minor axis): similar numbers of M31 halo stars given the 5:3 apparent flattening of the halo (Ferguson et al. 2002), but a larger number of M31 disk stars (Hodder 1995). This would nominally imply a *lower* galaxy contamination fraction in our G1 field assuming an isotropic

³IRAF is distributed by the National Optical Astronomy Observatories, which are operated by the Association of Universities for Research in Astronomy, Inc., under cooperative agreement with the National Science Foundation.

galaxy distribution. However, the RG02 spectroscopic sample was pre-screened against galaxies using *UBRI* photometry (Reitzel et al. 1998), in addition to standard morphological star-galaxy separation, whereas no such color selection is done in the present study. Thus, a higher fraction of galaxies may have slipped into our G1 field spectroscopic sample.

2. The remainder of the failures in the RG02 study are thought to be a result of inadequate S/N. The total exposure times for our G1 field spectroscopic masks are a factor of 2–3 shorter than for the RG02 masks. Based on tests using subsets of the RG02 data, we expect the failure rate due to inadequate S/N to be about 20% for the G1 field sample presented here.

2.4. Metallicity Estimation

The metallicity of each star is estimated from its position in the $(V - I, I)$ color-magnitude diagram Fig. 1, by comparing it to model isochrones from the Padova group (Girardi et al. 2000) with $[\text{Fe}/\text{H}] = -2.3, -1.7, -1.3, -0.7, -0.4, -0.02,$ and $+0.18$ and $t = 12.6$ Gyr. The isochrones are translated into apparent/observed I vs. $V - I$ space based on an adopted M31 distance of 783 kpc (Stanek & Garnavich 1998; Holland 1998), or a true distance modulus of $(m - M)_0 = 24.47$, and a mean reddening of $\langle E(B - V) \rangle = 0.06$ towards G1 derived from the Schlegel, Finkbeiner, & Davis (1998) dust map. A standard slope of $R_V = 3.1$ is assumed for the Galactic dust extinction law, which translates into $E(V - I)/E(B - V) = 1.4$ (Cardelli, Clayton, & Mathis 1989). The resulting model isochrones are fit with a Legendre polynomial of 6th order in $V - I$ and 10th order in I to interpolate between the isochrones. This yields a photometric estimate of each star’s metallicity, $[\text{Fe}/\text{H}]_{\text{phot}}$. If the actual age of the stellar population is closer to 4 Gyr instead of the value of 12.6 Gyr adopted in this paper (Rich et al. 2003), the metallicity estimates would be revised upwards by about +0.3 dex (see Fig. 1).

The errors in metallicity are dominated by systematics in the method. The relative metallicities of the sample may be ranked to within 0.1 dex, but the true metallicity of each star is uncertain by at least 0.25 dex due to systematic errors such as differential reddening, age error/spread, variations in the degree of alpha enhancement, and inaccuracies in the models. The systematic error of 0.25 dex is added in quadrature to a random error component of 0.1 dex: conservatively, our metallicities have overall errors on the order of 0.27 dex.

The above error estimates apply only to stars located within the range of the model isochrones in Fig. 1. It is clear from the CMD though that a significant number of stars lie above the tip of the RGB and/or are bluer than the most metal-poor isochrone. As discussed in §3, most of these outliers are foreground Galactic dwarf stars for which the $[\text{Fe}/\text{H}]_{\text{phot}}$ estimate is in any case meaningless. Two of the outliers are probable members of M31’s disk (see below); we caution that their extrapolated $[\text{Fe}/\text{H}]_{\text{phot}}$ estimates are very uncertain.

RG02 derive spectroscopic metallicity estimates from Ca II line strengths. The lower S/N of our spectra makes such estimates unreliable so they are not presented here. We have verified though that the gross features of the $[\text{Fe}/\text{H}]$ vs. radial velocity plot [Fig. 2 (bottom)] remain unchanged when the photometric metallicity estimates are replaced with spectroscopic ones.

3. Discussion

The distribution of heliocentric radial velocities in our sample shows a clear concentration near $v \simeq -450 \text{ km s}^{-1}$ and another near $v \simeq -75 \text{ km s}^{-1}$ [Fig. 2 (top)]. Based on this observed distribution, the sample can be crudely divided into three main components: Milky Way dwarf stars, M31 halo giants, and M31 disk giants. We expect that most of the 18 objects with $v \geq -200 \text{ km s}^{-1}$ are foreground Galactic dwarf stars (RG02; Ratnatunga & Bahcall 1985) and do not consider these for any further analysis.

Seven objects lie in the velocity range $-400 < v < -200 \text{ km s}^{-1}$. They are likely to be M31 field halo RGB stars, with some possibly representing tidal debris from G1. One star is potentially a member of the G1 globular cluster: it lies $30''$ from the cluster center, well within its tidal radius of $54''$ (Meylan et al. 2001) in projection; its metallicity $[\text{Fe}/\text{H}]_{\text{phot}} = -0.74$ is within the $\pm 1\sigma$ intrinsic $[\text{Fe}/\text{H}]$ spread (0.39 dex) around G1’s mean metallicity of -0.95 dex (Meylan et al. 2001); its radial velocity $v = -377 \text{ km s}^{-1}$ is within the $\pm 2\sigma$ intrinsic velocity dispersion ($\sigma_v = 28 \text{ km s}^{-1}$) around G1’s systemic velocity of $v = -331 \text{ km s}^{-1}$ (Meylan et al. 2001). Three of the remaining “halo-like” objects have velocities and metallicities which are within $\pm 1\sigma$ of G1’s values and two more lie within $\pm 2\sigma$ [Fig. 2 (bottom)]. However, none of these five stars are physically close to G1, the closest being more than two tidal radii away. These stars may represent tidal debris from G1; however the small size of our sample makes it impossible for us to draw any firm conclusions.

The remaining 16 objects with $v < -400 \text{ km s}^{-1}$ appear to be tightly clustered around a mean velocity of -451 km s^{-1} . This is similar to the velocity of the 21-cm neutral hydrogen line, $v_{\text{HI}} \sim -516 \text{ km s}^{-1}$ for the gaseous disk $10'$ due east of G1; however, no HI gas has been detected at the exact location of G1 (Thilker 2003). Sawa & Sofue (1982) fit a linear density-wave model (Lin, Yuan, & Shu 1969) to the mean rotation curve derived from the high-sensitivity HI survey by Cram, Roberts, & Whitehurst (1980) in order to construct a velocity field map of M31. Their model predicts a disk velocity of $v \simeq -455 \text{ km s}^{-1}$ at our field location (G1 is at a projected distance of $r \sim 34 \text{ kpc}$ from the galaxy center near its SW major axis). Sofue & Kato (1981) use the mean rotation curve observed for M31 and assume an inclination of $i = 77^\circ$ to construct a radial velocity field: this predicts a disk velocity of $v \simeq -480 \text{ km s}^{-1}$ near G1. Both predictions agree with our measured mean velocity to within the errors. A Gaussian centered at $v = -451 \text{ km s}^{-1}$ with $\sigma = 27 \text{ km s}^{-1}$ fits the distribution well [Fig. 2 (top)]. This observed velocity spread is roughly equivalent to (if slightly larger than) our estimated velocity measurement error. Subtracting the measurement error in quadrature from the measured dispersion yields an *intrinsic* dispersion of less than 20 km s^{-1} for the sample of “disk-like” RGB stars, although this value is not well constrained because of the small sample size. The rms velocity dispersion of the HI gas is measured to be 8.1 km s^{-1} independent of position within M31’s disk (Unwin 1983). Nolthenius & Ford (1987) find a velocity dispersion of about 38 km s^{-1} for a sample of M31 “disk” planetary nebulae located somewhat closer to the galaxy’s center ($15 < r < 30 \text{ kpc}$), but it is possible that some of these objects belong to the dynamically hotter halo or thick disk components.

These “disk-like” RGB stars near G1 have a mean metallicity of $\langle [\text{Fe}/\text{H}]_{\text{phot}} \rangle_{\text{disk}} = -0.8$. The $[\text{Fe}/\text{H}]$ distribution appears to be somewhat asymmetric: the peak is shifted towards the metal-rich end (-0.55 dex) with an extended tail towards metal-poor values [Fig. 2 (bottom)]. By contrast, the seven “halo-like” stars have a mean metallicity of $\langle [\text{Fe}/\text{H}]_{\text{phot}} \rangle_{\text{halo}} = -0.99$. It should be noted, however, that the metal-rich end of these distributions are not well constrained because the spectroscopic sample is magnitude-limited (RG02): the tip of the RGB is not as bright for a metal-rich population as it is for a metal-poor one and this leads to a bias against metal-rich stars. In addition, our demarcation between “halo” and “disk” samples at -400 km s^{-1} is arbitrary: it is possible that a small fraction of our “disk-like” stars actually belong to M31’s halo.

Our results on M31 outer disk stars can be compared to two other studies targeting the outer disks of spiral galaxies. Davidge (2003) finds mean metallicities of $\langle [\text{Fe}/\text{H}] \rangle \lesssim -1$ in the outer parts of the Sc galaxies M33 and NGC 2403. Ferguson, Gallagher, & Wyse (1998) find gas phase $[\text{O}/\text{H}]$ abundances that are roughly 10% solar in the far outer regions ($1.5 - 2 R_{25}$) of late-type disk galaxies; assuming a solar $[\text{O}/\text{Fe}]$ ratio, this gas would form stars with $[\text{Fe}/\text{H}] \sim -1$. The spiral galaxies in these studies are less luminous and of later Hubble type than M31, so it is perhaps not surprising that M31’s outer disk is more metal rich than theirs. In addition, the accompanying paper by Rich et al. (2003) describes stellar photometry in a deep *Hubble Space Telescope*/Wide Field Planetary Camera 2 field located only 2 kpc in projection from G1, and finds evidence for a population of objects with an age of 6–8 Gyr. Two of the disk-like stars in our spectroscopic sample lie well above the tip of the RGB (Fig. 1) and could be representative of an intermediate-age asymptotic giant branch population. This is consistent with the findings of the Davidge study. Thus, the cumulative evidence leads us to believe that the majority of metal-rich stars in our sample represents a population that formed in a disk. It is also possible, though less likely, that this population instead represents a merger event that happens to have the same radial velocity as the outer disk of M31.

4. Summary

We use Keck/LRIS multi-slit spectroscopy to measure the Ca near-infrared triplet in 41 candidate M31 giants in the apparent magnitude range $20 < I < 22$. We find 23 stars have radial velocities that are consistent with membership in M31; two-thirds of these M31 member candidates likely belong to a disk population. The disk stars have a mean heliocentric radial velocity of $v = -451 \text{ km s}^{-1}$. A Gaussian centered at this velocity with $\sigma = 27 \text{ km s}^{-1}$ fits the distribution indicating a true velocity dispersion in the disk of $\sigma_{\text{intrinsic}} < 20 \text{ km s}^{-1}$ (after accounting for velocity measurement error). This “disk-like” population has a mean metallicity of $[\text{Fe}/\text{H}] = -0.8$; most of the stars are slightly more metal-rich than this, with a tail to lower metallicities. Although the velocities and metallicities are consistent with a disk population, we cannot rule out the possibility that these stars belong to a dynamically-cold stream from a recent satellite merger event.

Six stars have metallicities and velocities that are roughly consistent with G1’s values. One of these stars lies within the tidal radius of G1 (at least in projection) and is thus likely to be a member of the globular cluster. The remaining five could possibly represent tidal debris from G1, but are more likely to simply be M31 field halo stars. Even if they do represent G1 tidal debris, they make up no more than 20% of the overall population, as most of the metal-rich stars in the field appear to belong to M31’s disk. A larger sample is needed in order to determine the exact contributions of these various populations to M31’s outer disk region.

Support for proposal GO-9099 was provided by NASA through a grant from the Space Telescope Science Institute, which is operated by the Association of Universities for Research in Astronomy under NASA contract NAS 5-26555. P.G. acknowledges support from the National Research Council of Canada in the form of a 2002-2003 Herzberg fellowship, and is grateful to the Herzberg Institute of Astrophysics for hosting him during that time. He would also like to thank Joe Miller for his support through a UCO/Lick Observatory Director’s grant. We thank Marla Geha for a careful reading of the manuscript. The authors wish to recognize and acknowledge the very significant cultural role and reverence that the summit of Mauna Kea has always had within the indigenous Hawaiian community. We are most fortunate to have the opportunity to conduct observations from this mountain.

REFERENCES

- Aurière, M. 1982, *A&A*, 109, 301
- Cardelli, J. A., Clayton, G. C., & Mathis, J. S. 1989, *ApJ*, 345, 245
- Choi, P. I., Guhathakurta, P., & Johnston, K. V. 2002, *AJ*, 124, 310
- Cram, T. R., Roberts, M. S., & Whitehurst, R. N. 1980, *A&AS*, 40, 215
- Davidge, T. J. 2003, *AJ*, 125, 3046
- Dolphin, A. E. 2000, *PASP*, 112, 1383
- Ferguson, A. M. N., Gallagher, J. S., & Wyse, R. F. G. 1998, *AJ*, 116, 673
- Ferguson, A. M. N., Irwin, M. J., Ibata, R. A., Lewis, G. F., & Tanvir, N. R. 2002, *AJ*, 124, 1452
- Ferguson, A. M. N., & Johnson, R. A. 2001, *ApJ*, 559, L13
- Girardi, L., Bressan, A., Bertelli, G., & Chiosi, C. 2000, *A&AS*, 141, 371
- Guhathakurta, P., & Reitzel, D. B. 2002, *BAAS*, 201, 14.11
- Hodder, P. J. C. 1995, Ph.D. thesis, University of British Columbia
- Holland, S. 1998, *AJ*, 115, 1916
- Holtzman, J. A., Burrows, C. J., Casertano, S., Hester, J. J., Trauger, J. T., Watson, A. M., & Worthey, G. 1995, *PASP*, 107, 1065
- Lin, C. C., Yuan, C., & Shu, F. H. 1969, *ApJ*, 155, 721
- Meylan, G., Sarajedini, A., Jablonka, P., Djorgovski, S. G., Bridges, T., & Rich, R. M. 2001, *AJ*, 122, 830
- Nolthenius, R., & Ford, H. C. 1987, *ApJ*, 317, 62
- Oke, J. B., Cohen, J. G., Carr, M., Cromer, J., Dingizian, A., Harris, F. H., Labrecque, S., Lucinio, R., Schaal, W., Epps, H., & Miller, J. 1995, *PASP*, 107, 385
- Phillips, A. C., et al. 2003, in preparation
- Ratnatunga, K. U., & Bahcall, J. N. 1985, *ApJS*, 59, 63
- Reitzel, D. B., & Guhathakurta, P. 2002, *AJ*, 124, 234
- Reitzel, D. B., Guhathakurta, P., & Gould, A. 1998, *AJ*, 116, 707
- Rich, R. M., Reitzel, D. B., Guhathakurta, P., Gebhardt, K., & Ho, L. C. 2003, *ApJ*, submitted
- Sawa, T., & Sofue, Y. 1981, *PASJ*, 33, 665
- Sofue, Y., & Kato, T. 1981, *PASJ*, 33, 449
- Schlegel, D. J., Finkbeiner, D. P., & Davis, M. 1998, *ApJ*, 500, 525
- Stanek, K. Z., & Garnavich, P. M. 1998, *ApJ*, 503, L131

Stetson, P. B. 1987, *PASP*, 99, 191

Thilker, D. 2003, private communication

Tonry, J., & Davis, M. 1979, *AJ*, 84, 1511

Unwin, S. C. 1983, *MNRAS*, 205, 773

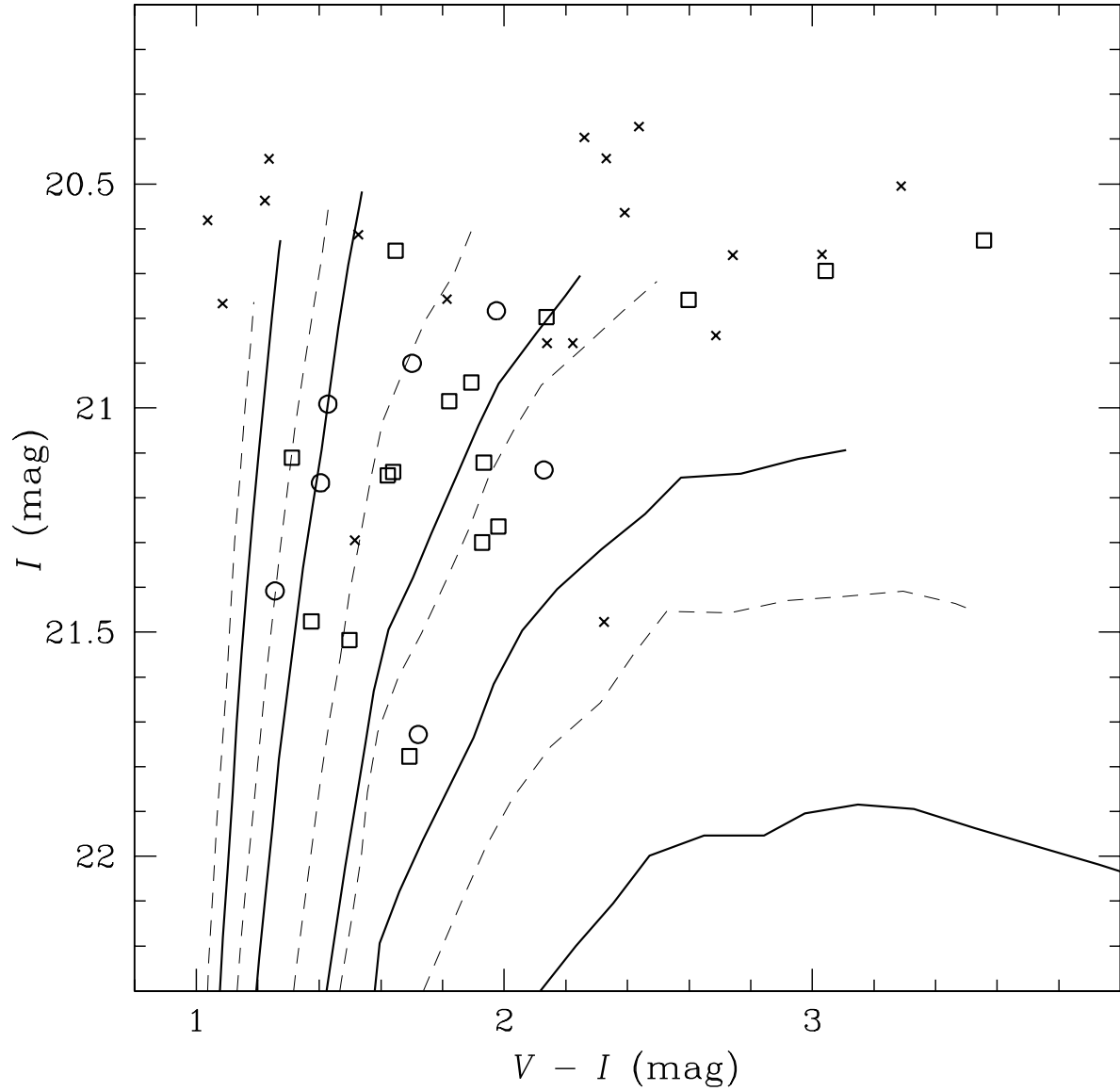


Fig. 1.— Color-magnitude diagram of the spectroscopic targets based on V and I photometry from LRIS and *HST*/WFPC2 images. Only the 41 targets for which a radial velocity measurement was possible are shown: $v > -200$ km s $^{-1}$ (“x”; likely foreground Milky Way dwarf stars); $-400 < v < -200$ km s $^{-1}$ (open circles); $v < -400$ km s $^{-1}$ (open squares; similar kinematics to the disk of M31). Isochrones from the Padova group (Girardi et al. 2000) with $[Fe/H] = -2.3, -1.3, -0.7, -0.4,$ and -0.02 (left→right) and $t = 12.6$ Gyr and $t = 4.0$ Gyr are shown as solid and dotted lines, respectively. Note, younger isochrones yield somewhat higher metallicity estimates for the stars.

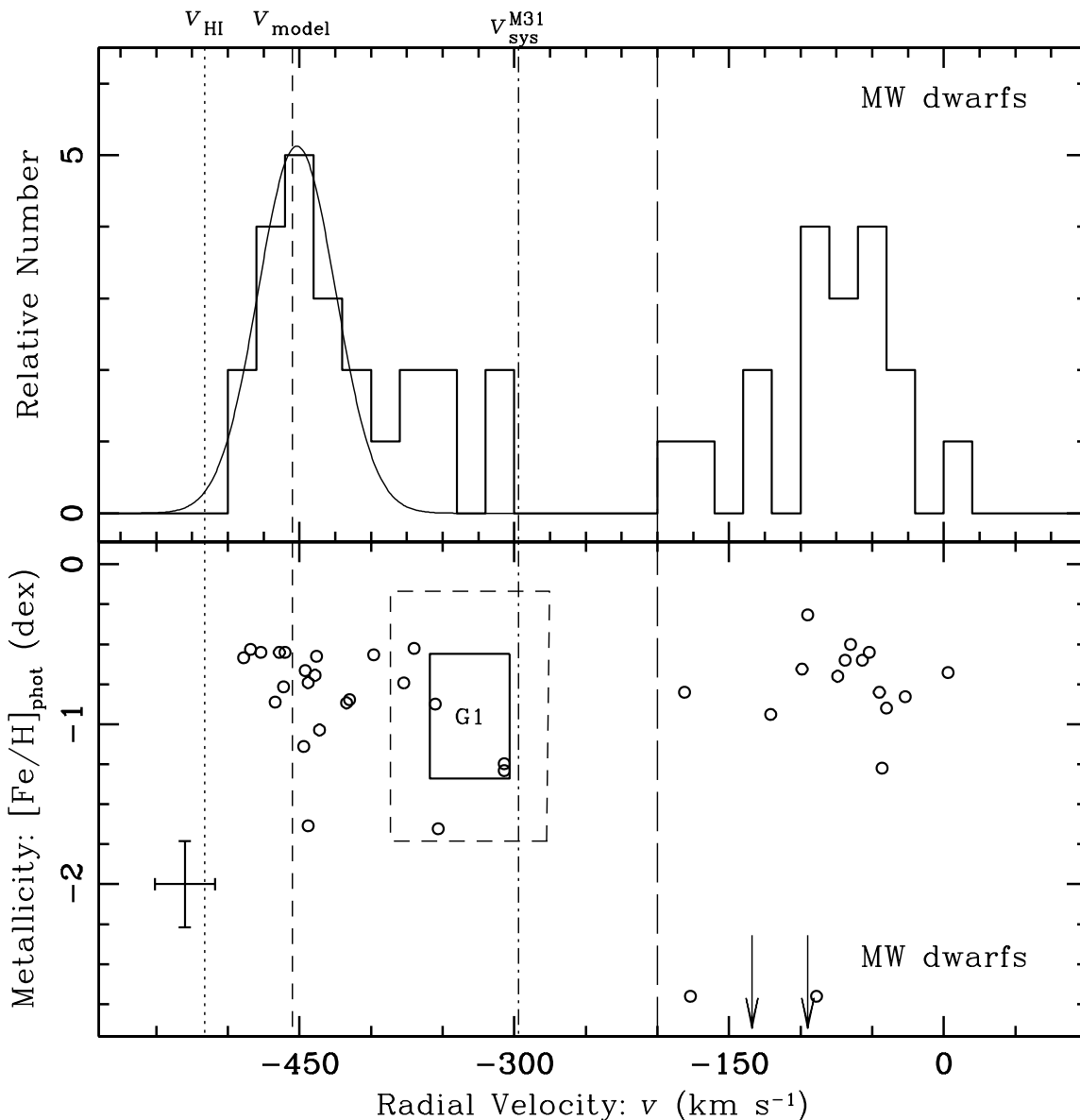


Fig. 2.— (*Top*) Distribution of heliocentric radial velocities for the main sample. The peak near $v \sim -75$ km s⁻¹ represents primarily Milky Way dwarf stars. The concentration near $v = -450$ km s⁻¹ is consistent with the velocity of M31’s HI disk 10’ east (dotted line) and especially with the model of M31’s velocity field along this specific line of sight (short-dashed line, Sawa & Sofue 1982), but not with the globular cluster G1 (see lower panel) or M31’s systemic velocity (dot-dashed line). Thus, these stars likely represent the M31 disk population and not tidal debris from G1. (*Bottom*) Radial velocity versus iron abundance, the latter estimated from each star’s position in the $(V - I, I)$ color-magnitude diagram (Fig. 1). Stars with $v > -200$ km s⁻¹ (long-dashed line) are likely to be Milky Way dwarf stars; the illustrated values of $[\text{Fe}/\text{H}]_{\text{phot}}$ for these objects are meaningless as the metallicity estimation method is only appropriate for M31 red giants. The $\pm 1\sigma$ measurement errors in radial velocity and metallicity are shown in the lower left. The solid and dashed rectangles indicate G1’s 1- σ and 2- σ (respectively) internal spread in metallicity and velocity (Meylan et al. 2001). Six objects lie within $\pm 2\sigma$ of G1’s values; one is a likely a member of the globular cluster as its projected position lies within G1’s tidal radius. The remaining five objects may represent tidal debris from G1 or may belong to M31’s smooth halo population; the majority of metal-rich stars in the field appear to belong to the disk of M31, not its halo.